A New BiRNN-SVA Method for Side Lobe Suppression

Shuyi Liu , Yan Jia, Yongqing Liu , Limin Zhai, and Xiangkun Zhang

Abstract—The spatially variant apodization (SVA) algorithm, a classic super-resolution method for synthetic aperture radar (SAR) images, can suppress side lobes while maintain the resolution of the main lobe. To address the problem of residual side lobes or loss of main lobe energy in improved SVA algorithms, the article proposes a new side lobe suppression method combining the bidirectional recurrent neural network (BiRNN) and the SVA algorithm, employing BiRNN to extract the main lobe and side lobe features of radar data to achieve side lobe suppression at any Nyquist sampling rate. The land flight experiment data of the fully polarized microwave scatterometer is used to quantitatively evaluate the side lobe suppression performance and the main lobe energy in order to verify the effectiveness of the BiRNN-SVA method. The experimental results demonstrate that the BiRNN-SVA method can be applied to data at any Nyquist sampling rate and has superior PSLR and ISLR compared to the GSVA algorithm and MSVA algorithm. The image processed with the proposed method retains more fine details and edge features. In comparison to the GSVA algorithm and MSVA algorithm, the image contrast and focus have increased by 31.6% and 3.6%, respectively, and by 4.4% and 1.1%.

Index Terms—BiRNN, side lobe, super resolution imaging, spatially variant apodization (SVA) algorithm.

I. INTRODUCTION

A S AN active microwave detection system, synthetic aperture radar (SAR) can perform high-resolution detection and imaging of the observation area at any time of day or night [1], and it plays an important role in military and civilian fields including terrain exploration, environmental monitoring, and electronic reconnaissance [2]. Improving resolution and optimizing image visual effects has always been a primary focus of radar imaging technology development [3]. In practical applications, high-resolution SAR images can clearly depict the scattering characteristics of targets, reducing the difficulty of interpreting radar images [4]. As the transmitting signal in SAR, the linear frequency modulation (LFM) waveform is typically adopted. The focused SAR image, however, exhibits high-brightness cross-like artifacts due to the finite support of the 2-D frequency domain, as the pulse response after matched filtering approximates a Sinc function with peak side lobe ratios (PSLR) as high as -13.26 dB [5]. In complex imaging scenes, the high-level side lobes of strong scattering targets can easily overwhelm the main lobe of weak targets [6], hindering the extraction of weak target information from SAR images and reducing the accuracy of target detection in subsequent image interpretation. In addition, high-level side lobes will also blur SAR images, decrease the contrast between adjacent targets, and visually weaken the distinction between targets [7]. To suppress the side lobe, an appropriate transmission waveform can be designed or a super-resolution imaging algorithm can be implemented. This article focuses primarily on the SAR image side lobe suppression algorithm from the perspective of image processing, with the goal of enhancing its weak target detection capability and image quality [8].

Existing methods for suppressing side lobes in SAR images include linear weighting and nonlinear weighting. The linear weighting method primarily suppresses the side lobe by introducing a classical window function in the frequency-domain matched filter, whereas frequency domain windowing will cause the main lobe to broaden while simultaneously suppressing the side lobe, resulting in a decline in the resolution [9]. To resolve the conflict between resolution and side lobe level, the nonlinear weighting method selects the minimum weighting result of the rectangular window and other weighting windows to determine the optimal weight for each pixel so as to suppress side lobes [10]. The SVA algorithm is a typical nonlinear weighting side lobe suppression method. It processes the real and imaginary parts of each pixel independently or simultaneously based on the cosine-based weighting function, effectively suppressing the side lobe while maintaining the width of the main lobe [11]. However, the traditional SVA algorithm is only applicable to data at integer multiples of the Nyquist sampling rate [12]. In cases of noninteger multiples of the Nyquist sampling rate or irregular point spread functions (PSFs) due to phase error distortion, the side lobe suppression effect of the SVA algorithm is weakened, severely restricting its practical application. As a result, several subsequent studies have proposed improved SVA algorithms. By modifying the frequency domain window function, the general SVA (GSVA) algorithm proposed in [13] is suitable for data at noninteger multiples of the Nyquist sampling rate, but there are still some side lobes. The robust SVA (RSVA) algorithm

The authors are with the Key Laboratory of Microwave Remote Sensing, National Space Science Center, Chinese Academy of Sciences, Beijing 100190, China, and also with the School of Electronic, Electrical and Communication Engineering, University of Chinese Academy of Sciences, Beijing 100049, China (e-mail: 919379957@qq.com; jiayan18@mails.ucas.ac.cn; 2624518773@qq.com; 985422574@qq.com; zhangxiangkun@mirslab.cn).

proposed in [14] uses a five-point filter and constraint theory to turn the weight optimization problem into a multi-vertex extremum problem in 2-D space. Although the RSVA algorithm can effectively suppress side lobes at any Nyquist sampling rate, it can result in energy loss in the main lobe and has a high level of complexity. By selecting effective points based on the RSVA algorithm, the modified SVA (MSVA) algorithm proposed in [15] further suppresses the side lobe and enhances the energy of the main lobe. It has a poor side lobe suppression effect in complex scenes, however, because of its nonmonotonic frequency domain filtering window. Liu et al. [16] proposes a double SVA algorithm suitable for squint SAR in an effort to solve the range-azimuth coupling issue of squint SAR. By introducing a displacement phase term, the side lobe in squint mode is corrected approximatively to side-looking mode, achieving side lobe suppression at any squint angle. Huan et al. [17] proposes a side lobe suppression method based on the wavelet transform and SVA algorithm that can further suppress side lobes and retain more image information without degrading the resolution of the main lobe. However, this method is currently applicable to data at integer multiples of the Nyquist sampling rate. Yuan et al. [18] proposes a side lobe suppression method combining the RSVA algorithm and a convolutional neural network, which can effectively increase the energy of the main lobe; nevertheless, the robustness of the algorithm is low because the model does not consider the correlation of the radar sequence data itself. The article proposes an adaptive weighted super-resolution imaging method that integrates BiRNN and SVA algorithm to suppress side lobes and better preserve main lobe energy at any Nyquist sampling rate.The main research contents include: In accordance with the range-compressed and azimuth-compressed signals of the Fourier imaging algorithm, generate data sets for suppressing side lobes via computer simulation; build a BiRNN-SVA side lobe suppression network and search for appropriate network training parameters; and using flight experiment data from the fully polarized microwave scatterometer, verify the effectiveness of the BiRNN-SVA method and compare it to the GSVA algorithm and MSVA algorithm to quantify the image improvement effect.

II. SPATIALLY VARIANT APODIZATION ALGORITHM

Based on a cosine-based weighting function, the SVA algorithm is a nonlinear method for suppressing side lobes. By selecting filter parameters based on data from neighboring sampling points, nonlinear filtering is accomplished. It compares the amplitudes of neighboring points, selects the minimum amplitude as the output for the current Nyquist sampling point, and effectively suppresses side lobes while retaining the original image resolution [19]. The weighting function for the first-order raised cosine in the frequency domain used in the SVA algorithm is

$$H(f) = 1 + 2\omega \cos\left(2\pi \frac{f}{f_s}\right)$$
$$-\frac{B}{2} \leq f \leq \frac{B}{2} \quad 0 \leq \omega \leq 0.5 \quad (1)$$

where ω denotes filter coefficient, B denotes the bandwidth of signals, and f_s is the sampling rate.

The mapping from the weighting in the frequency domain to the time domain is accomplished via convolution. For the real or imaginary part of the Nyquist sampling complex image $g(m)$, windowing in the frequency domain can be realized by three-point convolution in the time domain, and its expression in the time domain is

$$g'(m) = g(m) + \omega(m)g(m-1) + \omega(m)g(m+1). \quad (2)$$

When the image is sampled at integer multiples of the Nyquist sampling rate, the (2) becomes

$$g'(m) = g(m) + \omega(m)g(m-R) + \omega(m)g(m+R) \quad (3)$$

where $g(m)$ is the real or imaginary part of the original image, $g'(m)$ is the output of apodization filtering, $\omega(m)$ is the weighting coefficient, and $R = \frac{f_s}{B}$ denotes the multiple of Nyquist sampling.

To obtain the optimal side lobe suppression effect, the objective of parameter optimization is to minimize $|g'(m)|$ and solve for the optimal weighting coefficient $\omega(m)$ subject to $0 \leq \omega(m) \leq 0.5$. The SVA algorithm can be divided into two methods for complex Nyquist sampling images: joint processing of real and imaginary parts and separate processing of real and imaginary parts. When the real and imaginary parts are optimized jointly, the optimal weighting coefficient must exist on the modulus circle that is determined by the real and imaginary parts. At this time, the optimal weighting coefficient cannot ensure that both the real and imaginary parts attain the minimum value simultaneously. But if the real and imaginary parts are processed separately, the optimal weighting coefficients can be found so that both the real and imaginary parts reach the minimum value at the same time. This gives the algorithm a higher degree of freedom and makes the side lobe suppression effect better. Therefore, this section mainly introduces the SVA algorithm for the separation of real and imaginary parts.

Without taking into account the constraint condition $0 \leq \omega(m) \leq 0.5$, the optimal weighting coefficient solution is

$$\omega(m) = -\frac{g(m)}{g(m+R) + g(m-R)}. \quad (4)$$

Add constraint conditions, determine the minimum value of the real and imaginary parts, and acquire the output after apodization filtering as (5) shown at the bottom of the this page.

$$g'(m) = \begin{cases} g(m) & \omega(m) < 0 & (a) \\ 0 & 0 \leq \omega(m) \leq 0.5 & (b) \\ g(m) + 0.5 \times [g(m-R) + g(m+R)] & \omega(m) > 0.5 & (c) \end{cases}. \quad (5)$$

Let $y = [g(m - R) + g(m + R)]/2$ be the mean value of the adjacent points of $g(m)$. When $\omega(m) < 0$, $g(m)$ and y have the same sign, it can be ascertained that the current point is located in the main lobe, so $g(m)$ is not weighted to retain the main lobe. When $0 \leq \omega(m) \leq 0.5$, $g(m)$ and y have opposite signs, and $|g(m)| \leq |y|$, there must be a weight $\omega(m)$ to make $g'(m) = 0$ and zero out the side lobe energy. When $\omega(m) > 0.5$, $g(m)$ and y have opposite signs, and $|g(m)| > |y|$, the current point is in the main lobe region where the side lobe is superimposed, and $g'(m) = g(m) + y$ at this time. By applying (5) to the real and imaginary parts of the original Nyquist sampling image, the image after side lobe suppression processing can be obtained. The SVA algorithm is only applicable to data at integer multiples of the Nyquist sampling rate; consequently, several subsequent studies have proposed improved SVA methods, which can be divided primarily into two categories [20]: The first category of improved SVA algorithms is represented by the GSVA algorithm. By optimizing the frequency domain weighting function, the GSVA algorithm suppresses more side lobes than the SVA algorithm, but the image still contains a large number of side lobes. The second category of improved SVA algorithms, represented by the RSVA algorithm and the MSVA algorithm, increases the filter dimension from three to five points [21]. Based on polygonal constraints, these algorithms transform the optimization problem into a multivertex extremum problem. The RSVA algorithm and the MSVA algorithm use vertex-by-vertex calculations and linear programming, respectively, to determine whether a pixel belongs to main lobes or side lobes, achieving side lobe suppression at any Nyquist sampling rate. The primary drawbacks of these algorithms are energy loss in the main lobe and high computational complexity.

III. BiRNN-SVA METHOD FOR SIDE LOBE SUPPRESSION

The SVA algorithm is unsuitable for data at noninteger multiples of the Nyquist sampling rate, and the suppression effect in the case of PSF distortion is inadequate. There are issues with improved SVA algorithms, such as damaged main lobe energy and residual side lobes. In response, a new side lobe suppression method that combines the SVA algorithm and BiRNN is proposed in the article. The basic idea is to leverage the characteristics of BiRNN to capture contextual information and to derive the features of the main lobe and side lobe based on the adjacent pixel information of the radar data so as to effectively suppress the side lobe while maintaining the energy of the main lobe.

A. Generation of Dataset

The majority of classic SAR imaging algorithms (such as the RD algorithm, the CS algorithm, etc.) are founded on the theory of frequency domain matched filtering. The PSF of the focused SAR image is approximately a 2-D Sinc function. Therefore, the range-compressed and azimuth-compressed signals after pulse compression can be equivalent to a series of Sinc functions with
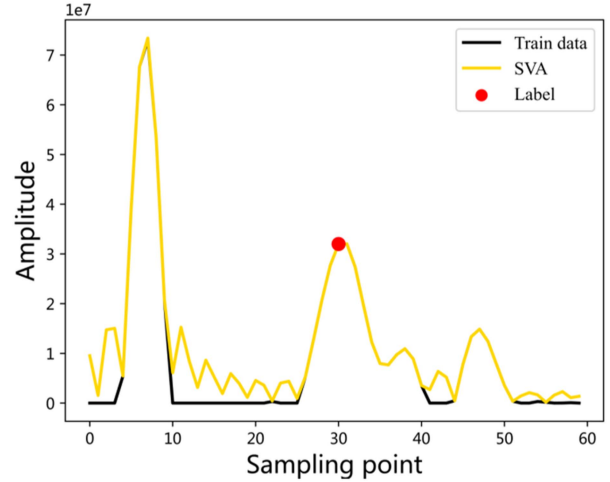

Fig. 1.   Samples from the training set.

varying delays [22], as shown in

$$s(n) = \sum_{i=1}^{N} \sigma_i e^{j\theta_i} \sin c\{KT(t - t_i)\} \qquad (6)$$

where N denotes the number of targets, K is the chirp rate of LFM waveforms, and T denotes the pulse duration, and t_i, σ_i, and θ_i, respectively, denote the echo delay, RCS, and phase of the ith point target.

1) Calculate the Nyquist sampling multiples in range and azimuth according to the range sampling rate, transmitted signal bandwidth, pulse repetition frequency (PRF), airborne flight speed, and reference distance, as shown in

$$R_{\text{range}} = \left\lfloor \frac{f_s}{B} \right\rfloor \quad R_{az} = \left\lfloor \frac{prf}{B_{az}} \right\rfloor \qquad (7)$$

where R_{range} is the multiple of the Nyquist sampling rate in range, R_{az} is the multiple of the Nyquist sampling rate in azimuth, B is the bandwidth of the transmitting signal, and B_{az} is the bandwidth of the signal in azimuth.

2) Generate a collection of target echo delays, RCS, and phase at random. Using (6), high side lobe echo data at integer multiples of the Nyquist sampling rate in range and azimuth are generated according to the bandwidth and multiple of the Nyquist sampling rate. The echo data with high side lobes is then truncated to L to serve as the training sequence. Here, $L = 20 \times R$, which is individually calculable based on the multiple of the Nyquist sampling rate in range and azimuth.

3) Set each training sequence's side lobes to zero with the SVA algorithm, and then choose the data at $\frac{L}{2}$ to serve as the label sequence of the training set, as shown in Fig. 1.

In order to evaluate accuracy and generalizability, the verification set employs practical data to analyze the performance of side lobe suppression. For 1-D data, the verification set chooses data along the horizontal direction via a sliding window whose length is L and whose sliding step is 1. After sliding over the entire data area and feeding it into the network, 1-D side lobe suppression results can be obtained. For 2-D SAR image data,
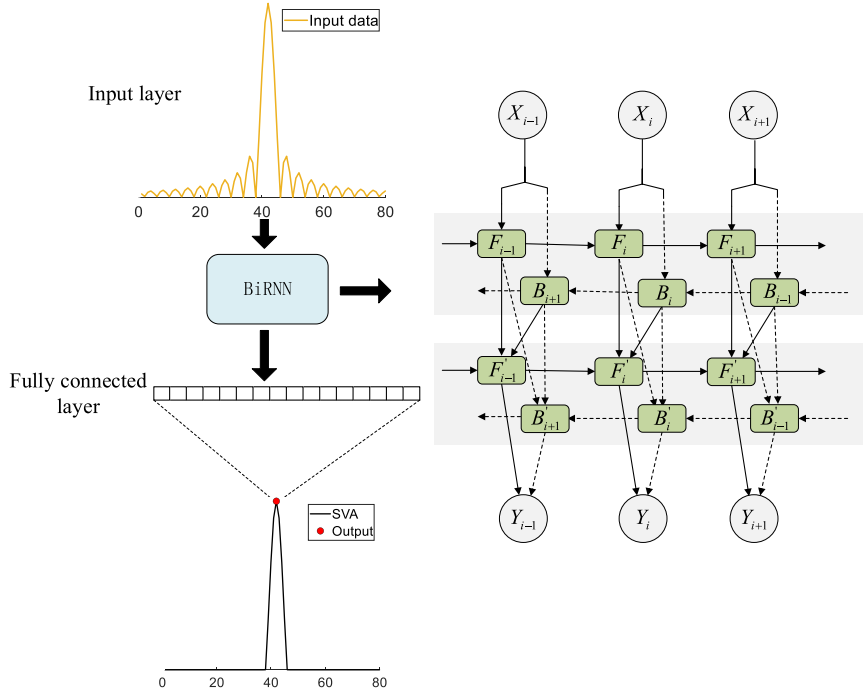
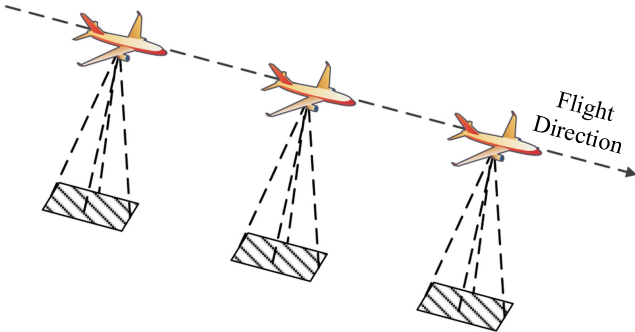Fig. 2. Structure of BiRNN-SVA sidelobe suppression network.

Fig. 3. Geometry of imaging observation.

the side lobes can be processed sequentially; that is, the range data is first input into the network for side lobe suppression, followed by the azimuth data.

B. Structure of Network

The primary characteristic of a recurrent neural network (RNN) is that the output of a neuron at a given time is used as the input of the neuron at the following time, allowing the network to learn the dependencies between sequence elements. In comparison to unidirectional RNN, the output of BiRNN at a given moment is not only related to the hidden state at the previous moment, but also related to the hidden state at the subsequent moment, allowing BiRNN to utilize contextual information for modeling and obtain more accurate results than RNN [23].

The input layer, BiRNN layer, and output layer make up the BiRNN-SVA network for side lobe suppression, shown in Fig. 2. The primary function of the input layer is to process

the loading order of the dataset in accordance with the network input requirements. The BiRNN layer contains six bidirectional hidden layers. The number of neurons is set to 30, and the rectified linear unit is chosen as the activation function in each hidden layer to enhance nonlinearity, thereby effectively enhancing the expressive ability of the network and preventing gradient disappearance. The output layer is a fully connected layer containing a neuron with the function of summarizing the temporal features derived by the BiRNN layer and predicting the output of the current pixel.

The input of the BiRNN-SVA network is the radar sequence data $X = \{X_1, X_2 \cdots X_t\}$, and the BiRNN contains a total of 6 BiRNN layers. Let $F_t^{(l)}$ and $B_t^{(l)}$ be the forward and backward hidden states of the lth layer at time t and the calculation equation is

$$F_t^{(l)} = \varphi(X_t W_F^{(l)} + F_{t-1}^{(l)} W_{Fh}^{(l)} + b_{Fh}^{(l)}) \tag{8}$$

$$B_t^{(l)} = \varphi(X_t W_B^{(l)} + B_{t+1}^{(l)} W_{Bh}^{(l)} + b_{Bh}^{(l)}) \tag{9}$$

where $W_F^{(l)}, W_{Fh}^{(l)}$, and $b_{Fh}^{(l)}$ are the weight matrix and bias vector of the forward layer, respectively, $W_B^{(l)}, W_{Bh}^{(l)}$, and $b_{Bh}^{(l)}$ are the weight matrix and bias vector of the forward layer respectively, and $\varphi(\text{·})$ is the activation function of the hidden layer

The temporal features of the radar sequence are obtained by splicing the hidden states $F_t^{(l)}$ and $B_t^{(l)}$ in both directions in the last BiRNN layer. The output layer calculates the output of the BiRNN-SVA network based on the temporal features, as depicted in (10), so that the predicted value at each time point completely incorporates past and future information of the input sequence
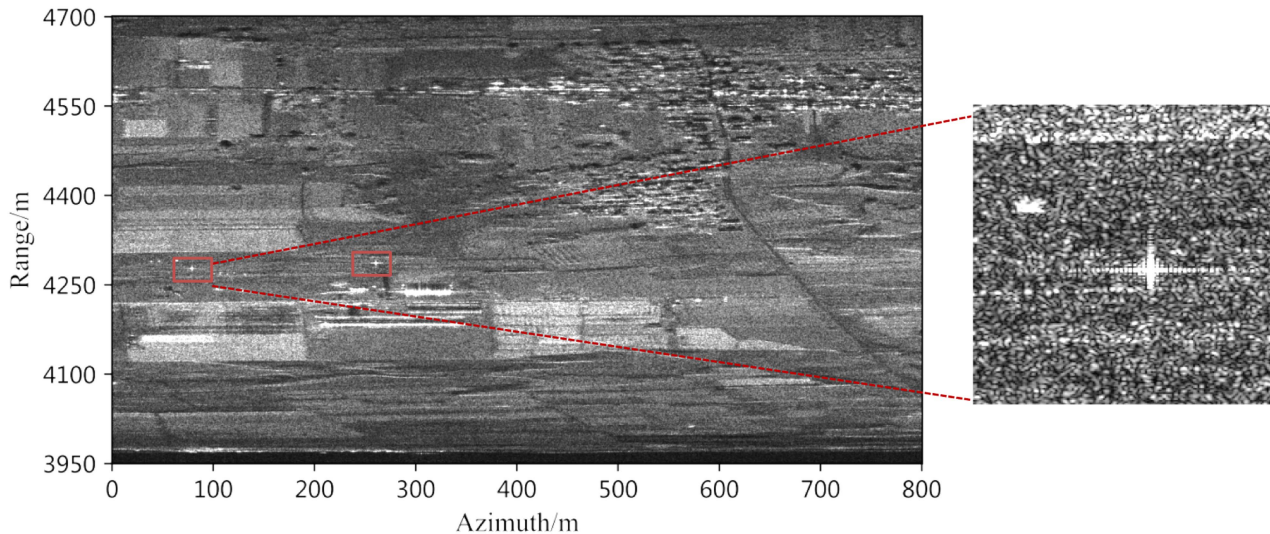
$$O_t = H_t W_{Hq} + b_q \tag{10}$$

Fig. 4.   Imaging results from the land flight experiment.

where O_t is the output of the BiRNN-SVA network, W_{Hq} and b_q are the weight matrix and bias vector of the output layer

C. Network Training

Training neural networks aims to determine the optimal weight parameters by minimizing the loss function [24]. Mean square error (MSE) is an appropriate loss function for regression problems. As shown in (11), the accuracy of the network is determined by calculating the expectation of the sum of squares of the distance between the predicted value and the actual value

$$\text{MSE} = \frac{1}{M} \sum_{i=1}^{M} (y_i - y_i') \tag{11}$$

where M represents the batch size, y_i represents the label value of the ith group in each batch, and y_i' represents the predicted output value [25]. The lower the MSE, the more accurate the network prediction [26].

To enhance the accuracy and convergence speed of the network, the small batch gradient descent optimization method is used to calculate and update the parameters during network training, with a batch size of 512. The learning rate adopts an adaptive adjustment strategy, and the adaptive moment estimation (Adam) optimization algorithm is used to adaptively adjust the learning rate of each parameter depending on the first-order moment and second-order moment estimation of the gradient, allowing the network to better fit the data and reduce gradient oscillation. The initial learning rate is set to 0.0001, and the decay rates of the first-order moment estimation and second-order moment estimation are, respectively, 0.90 and 0.99. Table I gives specific parameter configurations.

IV. VERIFICATION AND ANALYSIS OF EXPERIMENTS

In order to verify the application effect of the BiRNN-SVA side lobe suppression method in the practical SAR image, select

TABLE I
PARAMETERS OF NETWORK TRAINING

	Parameter	Value
Input layer	Input size	$1 \times L$
Output layer	Output size	1×1
Training parameters	Learning rate	0.0001
	Loss function	Mseloss
	Optimizer	Adam
	Batch size	512
	Epochs	100

PSLR, ISLR, image contrast (IC), and image entropy (IE) from the 1-D signal domain and 2-D image domain to quantitatively analyze the side lobe suppression performance and main lobe energy of SVA, GSVA, MSVA, and BiRNN-SVA methods [27].

A. Test Data

As one of the key payloads in airborne remote sensing systems, the fully polarized microwave scatterometer is an active microwave remote sensing device that works in two modes: high-precision backscatter measurement and high-resolution microwave imaging. It has potential applications in complex environmental observations and the multidimensional gathering of information [28]. From June 19 to June 28, 2019, the fully polarized microwave scatterometer conducted land and ocean flight experiments in Xi'an, Shanxi Province, and Dongying, Shandong Province, respectively. For the land flight experiment, the high-resolution imaging mode is utilized, and the scatterometer fixes the beam direction for frontal and side-looking observation. The observation area is the Dali calibration field in Xi'an's Yanliang District. Table II   and Fig. 3 show the
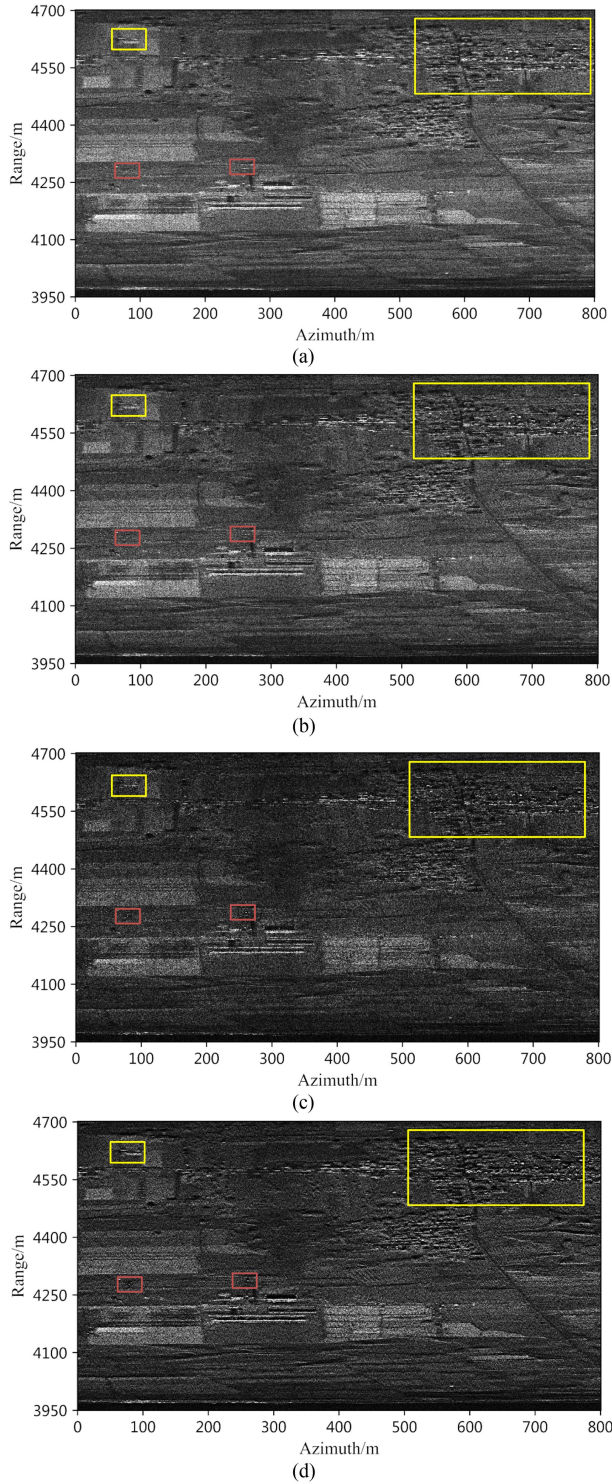
TABLE II
PARAMETERS OF NETWORK TRAINING

Parameter	Value
Operating frequency	13.4 GHz
Operating bandwidth	200 MHz
Pulse duration	10 us
Transmitting power	47 dBm
3 dB beamwidth	3°×20°
Sampling rate	400 M
PRF	500 Hz
Flight height	3 Km
Flight speed	350 Km/h

Fig. 5. Results of side lobe suppression for each method. (a) SVA. (b) GSVA. (c) MSVA. (d) BiRNN-SVA.

operational parameters of the system and the imaging geometry, respectively.

The imaging results from a specific region of the Dali calibration field using the range Doppler (RD) algorithm are shown in Fig. 4. The red box marks the location of a trihedral reflector with a side length of 0.5 m that was installed in the Dali calibration field. The processing for side lobe suppression will be carried out with this scene image.

B. Evaluation Indicator

To verify the performance of the BiRNN-SVA side lobe suppression method, PSLR, ISLR, IE, and IC are selected as evaluation indicators and compared with SVA, GSVA, and MSVA algorithms.

PSLR is defined as the intensity ratio of the maximum side lobe level to the main lobe, and ISLR is defined as the ratio of the total energy of the side lobe to the energy of the main lobe [29], as shown in

$$\mathrm{PSLR} = 20\log_{10}\left\{\frac{I_s}{I_m}\right\} \quad \mathrm{ISLR} = 10\log_{10}\left\{\frac{P_{\mathrm{total}} - P_m}{P_m}\right\} \tag{12}$$

where I_s represents the maximum side lobe level, I_m represents the main lobe level, P_{total} is the total energy of the signal, and P_m is the energy of the main lobe. If the PSLR and ISLR of impulse response are too high, the SAR image will display high-brightness cross-like artifacts, covering up the surrounding weak targets. The smaller the PSLR and ISLR, the more concentrated the energy distribution of the target, making weak targets easier to detect.

In SAR images, the function of IC is to measure the gray level difference or luminance between the target and the background and to quantitatively evaluate the clarity and visibility of the image. In general, a higher IC indicates that there is a distinct grayscale difference between the target and the background, which increases visibility and recognition of targets [30]. IE is an indicator to evaluate image focus. The lower the IE, the better the focus of the image; that is, the more distinct the boundaries and details of the target are. The methods for calculating IC and IE are shown as

$$\mathrm{IC} = \frac{\sqrt{E\left[|s(m,n)|^2 - E\left(|s(m,n)|^2\right)\right]^2}}{E\left(|s(m,n)|^2\right)} \tag{13}$$

$$\mathrm{IE} = -\sum_{m,n}\frac{|s(m,n)|^2}{E_s} \cdot \ln\left(\frac{|s(m,n)|^2}{E_s}\right) \tag{14}$$

where $s(m,n)$ is the pixel in the SAR image whose range index is m and azimuth index is n, and $E_s = \sum_{m,n}|s(m,n)|^2$, $E(\bullet)$ denotes the mean value operation.
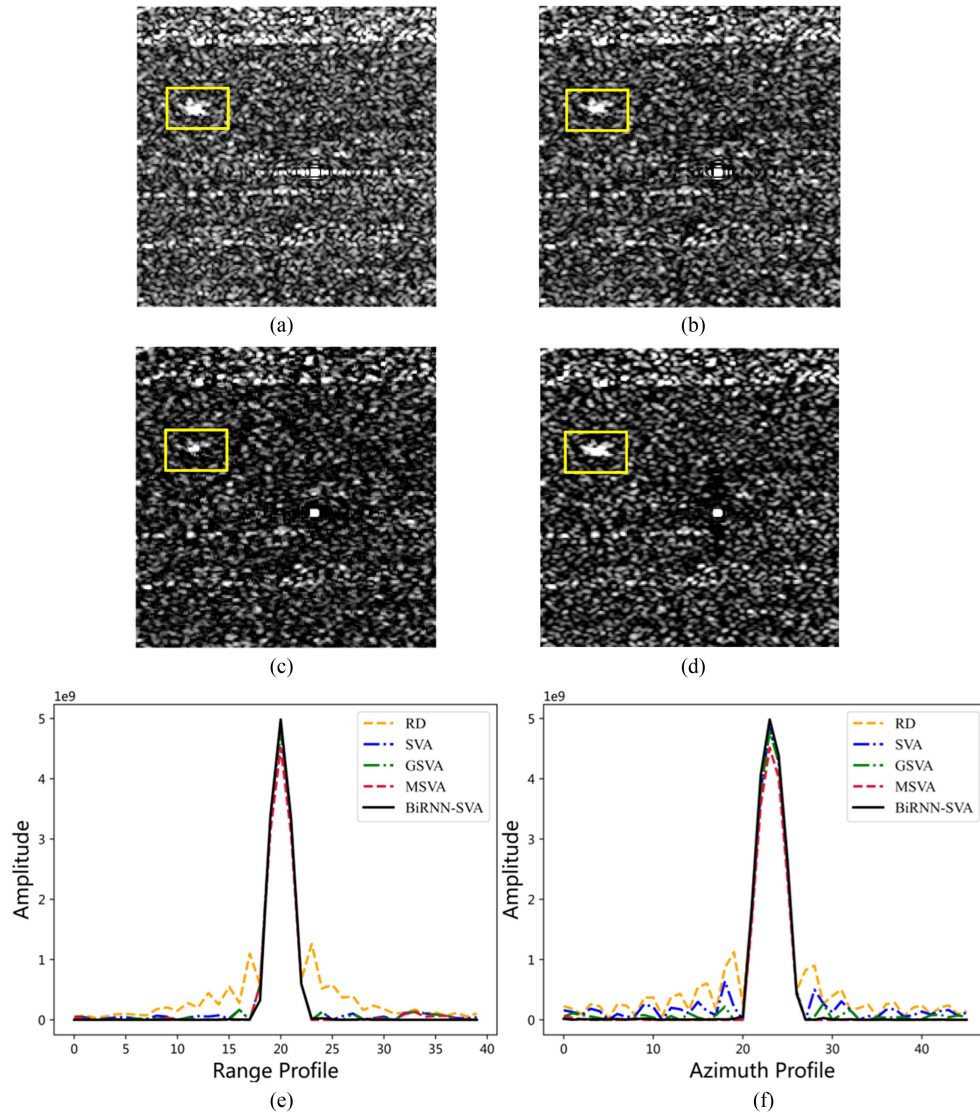
Fig. 6 Comparison of reflective corner region. (a) SVA. (b) GSVA. (c) MSVA. (d) BiRNN-SVA. (e) Range profile. (f) Azimuth profile.

C. Analysis of Experiment Results

Fig. 5 shows the results of SVA, GSVA, MSVA, and BiRNN-SVA methods for side lobe suppression of the land flight experiment image. By enlarging the region containing the corner reflector, it is simple to observe that the SVA algorithm effectively suppresses all side lobes in range and that the range-compressed signal in imaging mode is at integer multiples of the Nyquist sampling rate. The azimuth-compressed signal, however, corresponds to a noninteger multiple of Nyquist sampling. As depicted in Fig. 5(a), the side lobe suppression effect of the SVA algorithm decreases significantly, and there are some side lobes in azimuth. As shown in Fig. 5(b), the GSVA algorithm modifies the frequency domain window function to be suitable for noninteger multiples of Nyquist sampling, but the improvement effect on side lobe suppression in azimuth is limited, and there are residual side lobes in the case of noninteger multiples of Nyquist sampling. The MSVA algorithm accomplishes side lobe suppression at any Nyquist sampling rate by extending the dimension of the filter to five-point convolution, and it suppresses all side lobes in range and azimuth in the land flight experiment image. The range and azimuth profiles of the corner reflector indicate that the MSVA algorithm will lose the energy of the main lobe, which will significantly reduce the intensity of the image, resulting in the loss of edge and detail information about the target and increasing the difficulty of target detection and recognition [31].

Fig. 5(d) depicts the results of the BiRNN-SVA side lobe suppression method applied to the land flight experiment image. The side lobe in the region where the corner reflector is located is wholly suppressed in range and azimuth, demonstrating the effectiveness of the proposed method at any Nyquist sampling rate. The BiRNN-SVA side lobe method can better retain the energy of the main lobe while suppressing the side lobe in the profiles of Fig. 6(e) and (f). In comparison to the GSVA algorithm and MSVA algorithm, the range-compressed and

TABLE III
PERFORMANCE INDICATORS OF EACH METHOD

	Azimuth ISLR/dB	Azimuth PSLR/dB	Range ISLR/dB	Range PSLR/dB	IC	IE
RD	-10.71	-13.18	-10.00	-12.08	0.97	14.15
SVA	-15.30	-17.76	-24.86	-29.18	1.21	13.70
GSVA	-24.00	-29.03	-26.16	-30.70	1.33	13.51
MSVA	-40.66	-39.90	-30.15	-32.96	1.69	13.05
BiRNN-SVA	-41.11	-44.70	-45.46	-45.32	1.75	12.91

azimuth-compressed signals have superior PSLR and ISLR, enabling them to effectively ensure the clarity of 2-D images and the visibility of fine details. The MSVA algorithm loses a significant amount of target details while suppressing side lobes in complex observation areas. As an illustration, the intensity of the building region marked by the yellow box in Fig. 5 is substantially reduced after the MSVA algorithm has been applied, and the edge features are also weaker. Due to the loss of main lobe energy, the overall signal-to-noise ratio of the image is diminished. Comparatively, the BiRNN-SVA method is more effective at preserving the layer and edge characteristics of the building region. The image processed by the proposed method has richer texture and detail information overall, as shown in Table III; the IC increases by 31.6% and 3.6% relative to the GSVA algorithm and the MSVA algorithm, respectively; and the focus increases by 4.4% and 1.6%, respectively. On the basis of the preceding results, it can be proven that the BiRNN-SVA method is superior to the SVA algorithm and improved SVA algorithms in terms of side lobe suppression.

V. CONCLUSION

The SVA algorithm is a nonlinear side lobe suppression method based on a cosine-based weighting function that can suppress side lobes and maintain the resolution of the main lobe without prior knowledge. It is widely used in super-resolution image processing, ultrawideband SAR, and other fields. The SVA algorithm is inapplicable to data at noninteger multiples of the Nyquist sampling rate. Improved SVA algorithms, represented by GSVA and MSVA, modify the frequency domain window function or extend the convolution dimension to achieve side lobe suppression at any Nyquist sampling rate, but there are still problems such as residual side lobes and main lobe energy degradation. In response, the article proposes a novel method for side lobe suppression that combines the SVA algorithm and BiRNN. Computer simulation is used to generate the data set for side lobe suppression, and the main lobe and side lobe features of radar data are extracted based on the ability of BiRNN to capture contextual information so as to achieve side lobe suppression at any Nyquist sampling rate. To verify the effectiveness of the BiRNN-SVA method, the land flight experiment image of the fully polarized microwave scatterometer

is chosen to quantitatively evaluate the performance from the perspectives of ISLR, PSLR, IC, and IE and compared with SVA, GSVA, and MSVA algorithms. The experimental results show that the BiRNN-SVA method is applicable to data sampled at any Nyquist rate. Compared to the GSVA algorithm and MSVA algorithm, the BiRNN-SVA method exhibits superior PSLR and ISLR in the range and azimuth; the IE increases by 31.6% and 3.6%, respectively; and the focus is enhanced by 4.4% and 1.1%, respectively. The 2-D image as a whole displays enriched textures and finer details, confirming that the BiRNN-SVA method effectively suppresses side lobes while preserving the energy of the main lobe. In terms of side lobe suppression, it outperforms the improved SVA algorithms in practical data. Based on the results of the article, in the future, research on adaptive weighting super-resolution imaging algorithms will be conducted in an effort to suppress side lobes and enhance SAR image resolution.

REFERENCES

[1] E. Rodriguez and J. M. Martin, "Theory and design of interferometric synthetic aperture radars," *IEE Proc. F Radar Signal Process.*, vol. 139, no. 2, pp. 147–159, Apr. 1992, doi: 10.1049/ip-f-2.1992.0018.

[2] J. C. Curlander and R. N. Mcdonough, *Synthetic Aperture Radar: Systems and Signal Processing*, Hoboken, NJ, USA: Wiley, 1991.

[3] J. Huang, "Research on key algorithms of SAR image super-resolution enhancement," 2019.

[4] H. Yang and J. Wang, "Sidelobe suppression of SAR images by spectrum shaping," in *Proc. IEEE Int. Geosci. Remote Sens. Symp.*, 2022, pp. 1668–1671, doi: 10.1109/IGARSS46834.2022.9884635.

[5] P. Zhang and R. Yang, "A new SAR superresolution algorithm based on apodization extrapolation," in *Proc. IEEE Int. Geosci. Remote Sens. Symp.*, 2008, pp. IV-407–IV-410.

[6] Y. Wu, K. Fu, W. Diao, Z. Yan, P. Wang, and X. Sun, "Range sidelobe suppression approach for SAR images using chaotic FM signals," *IEEE Trans. Geosci. Remote Sens.*, vol. 60, pp. 1–15, 2022, Art. no. 5219915, doi: 10.1109/TGRS.2021.3137903.

[7] Q. Chen and J. Liu, "Depression of SAR image sidelobes based on combination of attributed scattering center model and spatially variant apodization," *J. Electron. Meas. Instrum*, vol. 34, no. 10, pp. 57–64, 2020, doi: 10.13382/j.jemi.B2003021.

[8] Z. Xu and Q. Shi, "Interference mitigation for automotive radar using orthogonal noise waveforms," *IEEE Geosci. Remote Sens. Lett.*, vol. 15, no. 1, pp. 137–141, Jan. 2018, doi: 10.1109/LGRS.2017.2777962.

[9] K. Yang, G. Liao, Q. Xu, and W. Wabg, "Improved SVA method for SAR sidelobe suppression," *Chin. J. Radio Sci.*, vol. 27, no. 6, pp. 1158–1165, Dec. 2012.

[10] Y. Huang et al., "Ship detection algorithm based on spatially variant apodization sidelobe suppression and order statistic-constant false alarm rate," *J. Radars*, vol. 9, no. 2, pp. 335–342, Apr. 2020.

[11] H. C. Stankwitz, R. J. Dallaire, and J. R. Fienup, "Nonlinear apodization for sidelobe control in SAR imagery," *IEEE Trans. Aerosp. Electron. Syst.*, vol. 31, no. 1, pp. 267–279, Jan. 1995, doi: 10.1109/7.366309.

[12] Z. Xu et al., "Effect analysis and spectral weighting optimization of sidelobe reduction on SAR image understanding," *IEEE J. Sel. Top. Appl. Earth Obs. Remote Sens.*, vol. 12, no. 9, pp. 3434–3444, Sep. 2019, doi: 10.1109/JSTARS.2019.2925420.

[13] B. H. Smith, "Generalization of spatially variant apodization to noninteger Nyquist sampling rates," *IEEE Trans. Image Process.*, vol. 9, no. 6, pp. 1088–1093, Jun. 2000, doi: 10.1109/83.846250.

[14] C. Castillo-Rubio, S. Llorente-Romano, and M. Burgos-Garcia, "Robust SVA method for every sampling rate condition," *IEEE Trans. Aerosp. Electron. Syst.*, vol. 43, no. 2, pp. 571–580, Apr. 2007, doi: 10.1109/TAES.2007.4285354.

[15] C. Ni, Y. Wang, X. Xu, C. Zhou, and P. Cui, "A SAR sidelobe suppression algorithm based on modified spatially variant apodization," *Sci. China Technol. Sci.*, vol. 53, pp. 2542–2551, Sep. 2010.

[16] M. Liu, Z. Li, and L. Liu, "A novel sidelobe reduction algorithm based on two-dimensional sidelobe correction using D-SVA for squint SAR images," *Sensors*, vol. 18, no. 3, Mar. 2018, Art. no. 783.

[17] R. Huan, Y. Tao, Y. Chen, P. Yang, and S. Bao, "SAR image sidelobe suppression method based on wavelet transform and spatial variant apodization," *J. Data Acquisition Process.*, vol. 34, no. 3, pp. 558–565, 2019.

[18] S. Yuan, Z. Yu, C. Li, and S. Wang, "A novel SAR sidelobe suppression method based on CNN," *IEEE Geosci. Remote Sens. Lett.*, vol. 18, no. 1, pp. 132–136, Jan. 2021, doi: 10.1109/LGRS.2020.2968336.

[19] X. Tian and R. Yang, "The analyzation of SAR image adaptive sidelobe reduction algorithms and experiments," *Remote Sens. Technol. Appl.*, vol. 3, pp. 148–153, 2002.

[20] Z. Xu, G. Gong, Y. Luo, and G. Li, "Application of improved spatial variant apodization algorithm through constrained optimization in sidelobe suppression," *Syst. Eng. Electron.*, vol. 44, no. 11, pp. 3298–3304, 2022.

[21] B. GUO, *Research On Sidelobe Suppression Algorithm for Squint SAR Imaging*. Xi'an, China: Master, Xidian Univ., 2021.

[22] R. Yang, *High Resolution Microwave Imaging*. Arlington, VA, USA: Nat. Defense Ind. Press, 2013.

[23] K. Qian, Y. Wang, P. Jung, Y. Shi, and X. X. Zhu, "Basis pursuit denoising via recurrent neural network applied to super-resolving SAR tomography," *IEEE Trans. Geosci. Remote Sens.*, vol. 60, pp. 1–15, 2022, Art. no. 4710015, doi: 10.1109/TGRS.2022.3221185.

[24] Y. Dai, T. Jin, H. Li, Y. Song, and J. Hu, "Imaging enhancement via CNN in MIMO virtual array-based radar," *IEEE Trans. Geosci. Remote Sens.*, vol. 59, no. 9, pp. 7449–7458, Sep. 2021, doi: 10.1109/TGRS.2020.3035064.

[25] M. Schutz, C. Decroze, M. Lalande, and B. Lenoir, "Neural networks to increase range resolution of FMCW radar," *IEEE Sens. Lett.*, vol. 4, no. 8, Aug. 2020, Art. no. 7003004, doi: 10.1109/LSENS.2020.3010015.

[26] Y. Bai, Y. Xiao, X. Hou, Y. Li, C. Shang, and Q. Shen, "SAR image despeckling with residual-in-residual dense generative adversarial network," in *Proc. IEEE Int. Conf. Acoust., Speech Signal Process.*, 2023, pp. 1–5, doi: 10.1109/ICASSP49357.2023.10096355.

[27] T. Xiong, S. Wang, B. Hou, Y. Wang, and H. Liu, "A resample-based SVA algorithm for sidelobe reduction of SAR/ISAR imagery with noninteger Nyquist sampling rate," *IEEE Trans. Geosci. Remote Sens.*, vol. 53, no. 2, pp. 1016–1028, Feb. 2015, doi: 10.1109/TGRS.2014.2332252.

[28] S. Liu, J. Yan, Z. Gao, X. Zhang, X. Long, and H. Liu, "Design and flight experiment of fully polarized microwave scatterometer system for aerial remote sensing system," *Syst. Eng. Electron.*, vol. 45, no. 11, pp. 3382–3390, 2023.

[29] Y. Qu, *Research On SAR Image Sidelobe Suppression and Image Quality Improvement*. Xi'an, China: Master, Xidian Univ., 2022.

[30] C. Wang, *Research On SAR Imaging Algorithm in High Squint Angle And Sidelobe Control Technique*. Xi'an, China: Xidian Univ., 2014.

[31] M. V. Perera, N. G. Nair, W. G. C. Bandara, and V. M. Patel, "SAR despeckling using a denoising diffusion probabilistic model," *IEEE Geosci. Remote Sens. Lett.*, vol. 20, pp. 1–5, 2023, Art. no. 4005305, doi: 10.1109/LGRS.2023.3270799.

Shuyi Liu received the B.S. degree in engineering from Shandong Normal University, Jinan, China, in 2019. She is currently working toward the Ph.D. degree in engineering with the National Space Science Center, Beijing, China.

Her research interests are super resolution microwave imaging and ultra wideband waveform synthesis technology.

Yan Jia received the B.S. degree in remote sensing science and technology from Shandong Agricultural University, Taian, China, in 2017. He is currently working toward the Ph.D. degree in engineering with the National Space Science Center, University of Chinese Academy of Sciences, Beijing, China.

His research interests include microwave remote sensing, radar system design, and signal processing.

Yongqing Liu received the B.S. degree in electronic information engineering from Henan Polytechnic University, Jiaozuo, China, in 2020. He is currently working toward the Ph.D. degree in engineering with the National Space Science Center (NSSC), University of Chinese Academy of Sciences, Beijing, China.

His research interests include microwave remote sensing, radar system design, signal processing.

Limin Zhai received the B.S degree in engineering from China University of Mining and Technology, Beijing, China, in 2021. She is currently working toward the Doctoral degree in engineering with National Space Science Center, Chinese Academy of Sciences, Beijing, China.

Her research interests include microwave remote sensing measurement technology, and microwave remote sensing radar image processing algorithms.

Xiangkun Zhang received the B.S. degree in engineering from Harbin Engineering University, Harbin, China, in 1994, and the M.S. and Ph.D. degrees in engineering from National Space Science Center (NSCC), Chinese Academy of Sciences, Beijing, China, in 2002 and 2007, respectively.

He is currently a Research Fellow and a Doctoral Director with NSSC. His research interests include microwave remote sensing imaging theory and technology, and microwave measurement technology.